HOKKAIDO UNIVERSITY

Title	Dynamical LEED analysis of Ni2P (0001)-1 x 1 : Evidence for P-covered surface structure
Author(s)	Hernandez, Alvin B.; Ariga, Hiroko; Takakusagi, Satoru et al.
Citation	Chemical Physics Letters, 513(1-3), 48-52 https://doi.org/10.1016/j.cplett.2011.07.055
Issue Date	2011-09-06
Doc URL	https://hdl.handle.net/2115/47105
Type	journal article
File Information	CPL513-1-3_48-52.pdf

1
2
3
4
5
6
7
8
9
10
11
12
13
14
15
16
17
18
19
20
21
22
23
24
25
26
27
28
29
30
31
32
33
34
35
36
37
38
39
40
41
42
43
44
45
46
47
48
49
50
51
52
53
54
55
56
57
58
59
60
61
62
63
64
65

Dynamical LEED Analysis of Ni$_2$P (0001)-1×1:

Evidence for P-covered Surface Structure

Alvin B. Hernandez[1], Hiroko Ariga[1], Satoru Takakusagi[1], Kumiko Kinoshita[2], Shushi Suzuki[3]

Shigeki Otani[4] , S. Ted Oyama[5] and Kiyotaka Asakura[1]

Catalysis Research Center, Hokkaido University, Kita 1-1,

Sapporo 001-0021 , Japan

[2]*Environmental Material Development, Material Research and Development Laboratory, Japan Fine Ceramics*

Center, Atsuta, Nagoya, 456-8587, Japan

[3]*Department of Crystalline Materials Science, Graduate School of Engineering, Nagoya University,*

Nagoya 464-8603, Japan

[4]*National Institute for Material Science, 1-1 Namiki, Tsukuba, Ibaraki 305, Japan*

[5]*Environmental Catalysis and Nanomaterials Laboratory, Department of Chemical Engineering, Virginia Tech,*

Blacksburg, VA 2406, USA and Department of Chemical Systems Engineering, The University of Tokyo,

Tokyo 113-8656 ,Japan

Abstract

Nickel phosphide (Ni$_2$P) is an emerging catalyst for hydrodesulfurization and other important environment- and energy-related catalytic reactions. To understand its high performance, the surface structure of a Ni$_2$P (0001) single crystal surface was investigated using dynamical LEED analysis. The obtained surface structure for Ni$_2$P (0001)-1×1 is a P-covered Ni$_3$P$_2$ structure (Ni$_3$P_P structure) as opposed to the expected bulk terminated surface structures. This paper discusses the driving force for the formation of the Ni$_3$P_P surface, which involves the minimization of the dangling bonds.

Recently, a promising catalysis of nickel phosphide (Ni_2P) was discovered for hydrodesulfurization reaction [1]. Ni_2P is a transition metal phosphide (TMP) that has physical properties, such as hardness and strength that are typical of ceramics, yet has electrical properties of metals, such as conductivity and the Hall coefficient. Ni_2P has excellent catalytic activities for hydrodesulfurization [1-8], hydrodenitrogenation [1,6-8], hydrodeoxygenation [1], hydrodechlorination [9-11], water-gas shift reaction [12] and hydrogen evolution reaction [13]. In order to understand the origin of its high catalytic performance, surface science research has been carried out on Ni_2P single crystal surfaces. However, even the most fundamental surface structure of Ni_2P (0001) remains unknown [3,14-17].

The bulk crystal structure of Ni_2P belongs to space group $P\bar{6}2m$ with a = b = 0.5859 nm and c = 0.3382 nm [18,19], as shown in Fig. 1. Along the [0001] direction, the bulk structure consists of two different alternating stoichiometric planes, namely Ni_3P and Ni_3P_2 (Fig. 1b and 1c). Previous DFT (density functional theory) studies showed that the Ni_3P_2 terminated surface is more stable than the Ni_3P terminated surface [3,14], whereas STM and PEEM studies showed that a substantial amount of the surface is also terminated with the Ni_3P structure [4,15,16]. In addition to the primitive (1×1) termination, Ni_2P (0001) surfaces also show 3/2×3/2 and √3×√3-R30° reconstructed surface structures [4,16,17].

In this paper, we resolved these contradictions in the Ni_2P (0001)-1×1 surface by using dynamical LEED analysis – a technique not only sensitive to the surface lattice structure but also to the atomic composition and position. The calculated results for the Ni_2P (0001)-1×1 surface is a P-terminated Ni_3P_2 surface. We also discussed a possible mechanism for the formation of such a unique surface structure and its relation to its surface stability and catalytic activity.

The Ni_2P (0001) surface was cleaned by sputtering with 0.5 keV Ar ions followed by annealing at 750 K for 2 h under UHV conditions to achieve sharp 1×1 LEED patterns (Fig. 1d). LEED measurements were performed at pressures of approximately 10^{-8} Pa and at room temperature. The intensities of the diffraction spots were measured by a computer controlled data acquisition system equipped with an intensified CCD video camera. Experimental LEED IV curves were generated from 50 to 180 eV with 1 eV steps from the 1×1 diffraction patterns of the Ni_2P surface. For each equivalent beam, the IV curve was averaged, producing four non-equivalent sets of integer order beams, i.e., (1,0), (1,1), (−1,−1) and (2,0), with a total energy range $\Delta E = $ 484 eV.

The full dynamical LEED analysis was carried out using the Symmetrized Automated Tensor LEED (SATLEED) package [20-23]. Seven relativistic phase shifts were used; the Debye temperature from the DFT calculation was set at 700 K, and the real and imaginary parts of the complex inner potential (V_{or} and V_{oi}) were set at 10 and −5 eV, respectively. The real part of the complex inner potential was refined.

Two model structures were initially considered for the SATLEED calculation, namely the Ni_3P and the Ni_3P_2 models, which correspond to the two bulk terminated structures. The theoretical IV curves of these model structures were calculated and compared with the experimental IV curves using the Pendry reliability factor (R_p). The determination of the number of layers necessary for optimization was performed using the Hamilton ratio method [24-26]. The variance of R_p (RR) was equal to 0.29 (RR= $\sqrt{(8\,|\,Voi\,|\,/\Delta E)}$) [23]. The error estimation was carried out by changing each fitting parameter from the optimized values until the obtained R_p exceeds the minimum $R_p \times (1 + RR)$[23].

Figure 2 shows calculated IV curves of Ni_3P and Ni_3P_2 model structures from dynamical LEED analysis together with the experimental curve. The Ni_3P and Ni_3P_2 model structures gave R_p values of 0.33 and 0.35, respectively, after optimization up to the 4th layer. In addition, in order to account for the coexistence of Ni_3P- and Ni_3P_2-terminated structures on the Ni_2P (0001)-1×1 surface [12,15,16], dynamical LEED analysis based on the two-phase models of both surfaces with various compositions was also performed. Fig. 2c shows the best fitted IV curve of the combined Ni_3P- and Ni_3P_2-terminated structures (ratio of Ni_3P to Ni_3P_2 is 0.65 to 0.35). However, the R_p value for this two-phase model was not improved significantly (R_p = 0.29). We continued our investigation in order to find other model structures though R_p values of these 3 model structures were less than the lower limit of uncorrelated model, 0.43 = 1 - 1.96 RR [23].

We examined other surface structure models that were consistent with the surface space group of the LEED pattern (i.e., p31m), but with modified surface compositions. Four top-layer structures with different surface compositions were proposed as shown in Fig.3:

Ni_3P_Ni model – Ni_3P-terminated surface without the surface P (Ni-covered Ni_3P_2);

$Ni_3P_2\_Ni$ model – Ni_3P_2-terminated surface without the surface P (Ni-covered Ni_3P);

Ni_3P_P model – Ni_3P-terminated surface without the surface Ni (P-covered Ni_3P_2); and

$Ni_3P_2\_P$ model – Ni_3P_2-terminated surface without the surface Ni (P-covered Ni_3P).

In these model structures, the topmost atoms are regarded as the adatom on the 0th layer, and could be optimized up to the 3rd layer of surface structure according to the Hamilton ratio evaluation with a significance level of 10%[24].

As shown in Fig. 4, the Ni_3P_P model gave the lowest R_p value (0.18) while the other three model structures, Ni_3P_Ni, $Ni_3P_2\_P$ and $Ni_3P_2\_Ni$ had R_p values of 0.30, 0.33 and 0.32, respectively. Given the total number of peak, N = 24 and the fitting parameters of 11, 11, 12 and 12 for Ni_3P_P, Ni_3P_Ni, $Ni_3P_2\_P$ and $Ni_3P_2\_Ni$ models, respectively, F-test results for the R_p values showed that the Ni_3P_P was the most appropriate model with a confidence level of 96% when compared to the next best structure (Ni_3P_Ni).

This Ni_3P_P model structure can account for the STM image previously assigned to the "Ni_3P" surface structure (i.e. bright spot separation of approximately 0.59 nm). However, another surface structure appearing as "Ni_3P_2" was also reported in the same STM study [16]. Thus, a two-phase model composed of a Ni_3P_P and a "second surface structure" that gives similar surface geometry to the "Ni_3P_2" (i.e., a bright spot separation of about 0.34 nm) was calculated. The elaborate calculations showed that several two-phase model structures have improved R_p values but the dominant structure was always that of the Ni_3P_P structure with a percentage contribution of $80 \pm 10\%$. Although the "second surface structure" could not be determined by dynamical LEED analysis alone, we propose that the minor surface structure is likely to be the Ni_3P_2 structure because of the following reasons: 1) dynamical LEED calculation of the Ni_3P_P and Ni_3P_2 combined model structure gave one of the best R_p values (0.16); 2) the Ni_3P_P model structure – the most dominant structure – can easily be achieved by adsorbing P atoms on the Ni three-fold hollow site of Ni_3P_2; 3) the P atoms on the Ni_3P_2 model structure gives the bright spots in the STM image [16] of "Ni_3P_2"; and 4) previous DFT calculations [3] provide evidence that the Ni_3P_2-terminated surface is a stable surface structure. Thus, we tentatively conclude that the Ni_2P (0001)-1×1 surface is composed of approximately 80% Ni_3P_P (Ni_3P_2 covered with P at the Ni three-fold hollow sites) and 20% bare Ni_3P_2.

The details of the Ni_3P_P model structure, which is the dominant part of the Ni_2P (0001) surface, is illustrated in Fig. 5. The structural parameters with the calculated errors are listed in Table 1. The Ni_3P_P structure can be regarded as P adatoms present on the Ni_3P_2 surface, where the topmost P atoms (0th layer) were shifted a little downward by 0.01 Å while the P atoms in the 1st layer were shifted upward by 0.07 Å. In other words, the surface was terminated with P atoms. An XPS study showed that the surface core level shifts were only observed as P 2p XPS spectra [27]. This finding is consistent with our Ni_3P_P model structure where Ni atoms on the surface are covered with P atoms.

The question that arises from these results is; why does the Ni_3P_P appear? Given the preparation conditions that we have done in the experiment, a Ni rich surface composition was expected since sputtering selectively removes the phosphorus while annealing recovers the surface P/Ni ratio by P diffusion from the bulk [5,16]. Considering the 0th and 1st layer of Ni_3P_P, the average P/Ni ratio = 1. Thus, the Ni_3P_P is quite an unexpected surface structure. We explained the formation mechanism of Ni_3P_P as follows. DFT calculations reported that the Ni_3P_2 structure was more stable than the Ni_3P structure. When the Ni_3P_2 layer is exposed at the surface, each Ni three-fold site lacks one P atom on top thereby creating a dangling bond which has an energy around the Fermi level and generally makes the surface less stable [28]. Conversely, P atoms have a valence electron configuration of $3s^2 3p^3$. When P is adsorbed on the Ni three-fold hollow site in Ni_3P_2, the dangling bonds of the Ni atoms can be replaced with one fully occupied P lone pair which is located below the Fermi level, thus stabilize the surface.

Consequently, the surface is covered with P atoms. Similar P-terminated surface reconstructions were observed in Ni_2P $(10\bar{1}0)$ where the surface was reconstructed to $Ni_2P(10\bar{1}0)$-c(2×4) by the addition of P atoms on top of the exposed Ni sites [29]. These stabilization mechanisms are similar to those on semiconductor surfaces where the principle of the minimization of dangling bonds is manifested [28]. Thus, the mechanism for stable surface structure involving the "minimization of dangling bonds" is also valid in Ni phosphide surfaces.

Finally, we comment on the relation between the surface structure and catalysis. The surface of Ni_2P catalysts are preferentially covered with an oxygen chemisorption layer (passivation) in order to prevent bulk oxidation when handled under ambient conditions [1, 30]. The catalysts are then reduced prior to catalysis studies to remove the passivation oxygen. However, for these reduced Ni_2P catalysts, the exposed metal atoms measured by the chemisorption of CO was about 10–20% of the theoretical number estimated from the particle size [31]. The chemisorption amount decreased as the initial Ni/P ratios were decreased from 2/1 to 1/3. This observation indicated that the reduction in the chemisorption amounts was because of phosphorus blockage. The present study presents evidence for this explanation.

In summary, we conducted dynamical LEED analysis of the 1×1 surface of Ni_2P (0001) to resolve discrepancies between previously obtained STM data and DFT calculations. We found that the surface was mostly (~80%) terminated with Ni_3P_P structure (the P atom was adsorbed on the three-fold sites of Ni_3P_2). We conclude that the P adatoms further stabilize the Ni_3P_2 structure by filling the dangling bonds. The dangling bond minimization principle is valid for the nickel phosphide surfaces.

Figure captions

FIG. 1. a) Bulk structure of Ni_2P illustrating the alternating planes of Ni_3P and Ni_3P_2 along the [0001] direction; b) Ni_3P plane; c) Ni_3P_2 plane. Large and small balls correspond to the P and Ni atoms, respectively. d) The LEED pattern of Ni_2P (0001)-1×1 at 76 eV inserted with the reciprocal unit cell.

FIG. 2. Theoretical IV curves of the optimized a) Ni_3P, b) Ni_3P_2, c) two-phase Ni_3P-Ni_3P_2 (0.65:0.35) model structures compared with the experimental IV curve of Ni_2P (0001)-1×1.

FIG. 3. The top view of the 0th and 1st layer of Ni_2P (0001)-1x1 model structures satisfying the surface space group p31m but having a different composition. a) Ni_3P_P, b) Ni_3P_Ni, c) $Ni_3P_2\_Ni$ and d) $Ni_3P_2\_P$ model structures.   Circles indicate the added 0th layer atoms.

FIG. 4. Theoretical IV curves of the optimized a) Ni_3P_P, b) Ni_3P_Ni, c) $Ni_3P_2\_Ni$ and d) $Ni_3P_2\_P$ model structures compared with the experimental IV curve of Ni_2P (0001)-1×1.

FIG. 5. a) The side view of the optimized Ni_3P_P; b) the top view of the 0th to 1st layer (squared part in (a)). Arrows show the direction of the atomic displacement from the bulk position.

References

[1] S.T. Oyama. J. Catal. 216 (2003) 343.

[2] S.T. Oyama, X. Wang, Y.K. Lee, and W.J. Chun, J. Catal. 221 (2004) 263.

[3] P. Liu, J.A. Rodriguez, T. Asakura, J. Gomes, and K. Nakamura, J. Phys. Chem. B 109 (2005) 4575.

[4] M.G. Moula, S. Suzuki, W.J. Chun, S.T. Oyama, K. Asakura, and S. Otani, Surf. Interface Anal. 38 (2006) 1611.

[5] D. Kanama, S.T. Oyama, S. Otani, and D.F. Cox , Surf. Sci. 552 (2004) 8.

[6] Y.K. Lee, Y. Shu, and S.T. Oyama, Appl. Catal. A 322 (2007) 191.

[7] Y.K. Lee, and S.T. Oyama, J. Catal. 239 (2006) 376.

[8] S. Yang, C. Liang, and R. Prins, J. Catal. 237 (2006) 118.

[9] J. Chen, Y. Chen, Q. Yang, K. Li, and C. Yao. Cat. Comm. 11 (2010) 571.

[10] X.G. Liu, J.X. Chen, and J.Y. Zhang, Ind. Eng. Chem. Res. 47 (2008) 5362.

[11] S. Zhou, J. Chen, X. Liu, and J. Zhang, Chinese J. Cat. 28 (2007) 498.

[12] P. Liu, J.A. Rodriguez, Y. Takahashi, and K. Nakamura, J. Catal. 262 (2009) 294.

[13] P. Liu, and J.A. Rodriguez, J. Am. Chem. Soc. 127 (2005) 14878.

[14] Q. Li, and X. Hu.Phys. Rev. B. 74 (2006) 035414.

[15] M. G. Moula, S. Suzuki, W. J. Chun, S. Otani, S. T. Oyama, and K. Asakura, Chem.Lett35 (2006) 90.

[16] S. Suzuki, G.M. Moula, T. Miyamoto, Y. Nakagawa, K. Kinoshita, K. Asakura, S.T. Oyama, and S. Otani, J. Nanosci. and Nanotech. 89 (2008) 195.

[17] K. Kinoshita, G.H. Simon, T. Konig, M. Keyde, H-J. Freund, Y. Nakagawa, S. Suzuki, W.J. Chun, S.T. Oyama, S. Otani, and K. Asakura, Jap. J. Appl. Phys. 47 (2008) 6088.

[18] S. Rundqvist, Acta Chem. Scandi.16 (1962) 992.

[19] K. Adachi, and S. Ogawa, Landolt-Börnstein New Series III 27a (1988) 232.

[20] A. Barbieri, and M.A. Van Hove, Symmetrized Automated Tensor LEED (SATLEED) package, <http://www.ap.cityu.edu.hk/personal-website/Van-Hove_files/leed/leedpack.html>.

[21] M.A. Van Hove, W. Moritz, H. Over, P.J. Rous, A. Wander, A. Barbieri, M. Materer, U. Starke, and G.A. Somorjai, Surf. Sci. Rep.19 (1993) 191.

[22] P.J. Rous, Prog. Surf.Sci. 39 (1992) 3.

[23] J.B. Pendry, J. Phys. C: 13 (1980) 937.

[24] W.C. Hamilton, Acta. Cryst.18 (1965) 502.

[25] C. F. Walters, McCarty.K.F, E. A. Soares, and M. A. Van Hove, Surf.Sci. 464 (2000) L732.

[26] M.-S. Chen, S. Mizuno, and H. Tochihara, Surf. Sci., 536 (2003) L415.

[27] K. Edamoto, Y. Nakadai, H. Inomata, K. Ozawa, and S. Otani, Sol. State Comm. 148 (2008) 135.

[28] C.B. Duke, Chem. Rev. 96 (1996) 1237.

[29] D. Guo, Y. Nakagawa, H. Ariga, S. Suzuki, K. Kinoshita, T. Miyamoto, S. Takakusagi, K. Asakura, S. Otani, and S.T. Oyama, Surf. Sci. 604 (2010) 1347.

[30] A. E. Nelson, M. Y. Sun, and A. S. M. Junaid, Journal of Catalysis 241 (2006) 180.

[31] S. T. Oyama, X.Wang, Y.-K. Lee, K. Bando, and F. G. Requejo, J. Catal. 210 (2002) 207.

Table 1. Structural parameters with calculated errors for the optimized Ni₃P_P model structure.

Composition		Δz [001]	Δ(P-Ni bond)	Δ(Ni-P bond)	Δ(Ni-Ni bond)
0th layer	P	0.01±0.04	-	-	-
0th to 1st	P - Ni₃P₂	-	-0.03(2.24)±0.11	-	-
1st layer	P in Ni₃P₂	-0.07±0.05	0.01(2.22)±0.15		-0.03(2.59)±0.21
	Ni in Ni₃P₂	-0.01±0.05			
1st to 2nd	Ni₃P₂ - Ni₃P	-	0.08(2.54)±0.19	-0.00(2.26)±0.11	-0.01(2.60)±0.23
2nd layer	P in Ni₃P	0.00±0.06	-0.14(2.23)±0.26		0.09(3.17)±0.37
	Ni in Ni₃P	0.00±0.04			
2nd to 3rd	Ni₃P - Ni₃P₂	-	-0.04(2.23)±0.15	0.04(2.49)±0.20	-0.02(2.59)±0.26
3rd layer	P in Ni₃P₂	0.00±0.06	0.04(2.25)±0.20		-0.10(2.51)±0.28
	Ni in Ni₃P₂	0.00±0.09			

Notes:

a) For the z displacements, + and − values correspond to the inward and outward shifts normal to the surface;

b) For n^{th} to $(n+1)^{th}$ layer; the "P-Ni bond" means the P atom in the nth layer to the Ni atom in the $(n+1)^{th}$ layer;

c) For the Ni₃P₂ layer – the P-Ni bond and the Ni-Ni bond are 2.21 and 2.61 Å, respectively;

d) For the Ni₃P layer – the P-Ni bond and the Ni-Ni bond are 2.37 and 3.09 Å, respectively; and

e) For the Ni₃P to Ni₃P₂ (or Ni₃P₂ to Ni₃P) interlayer – the P-Ni (Ni-P) bond, Ni-P (P-Ni) bond and Ni-Ni (Ni-Ni) bond are 2.27, 2.46 and 2.61 Å, respectively
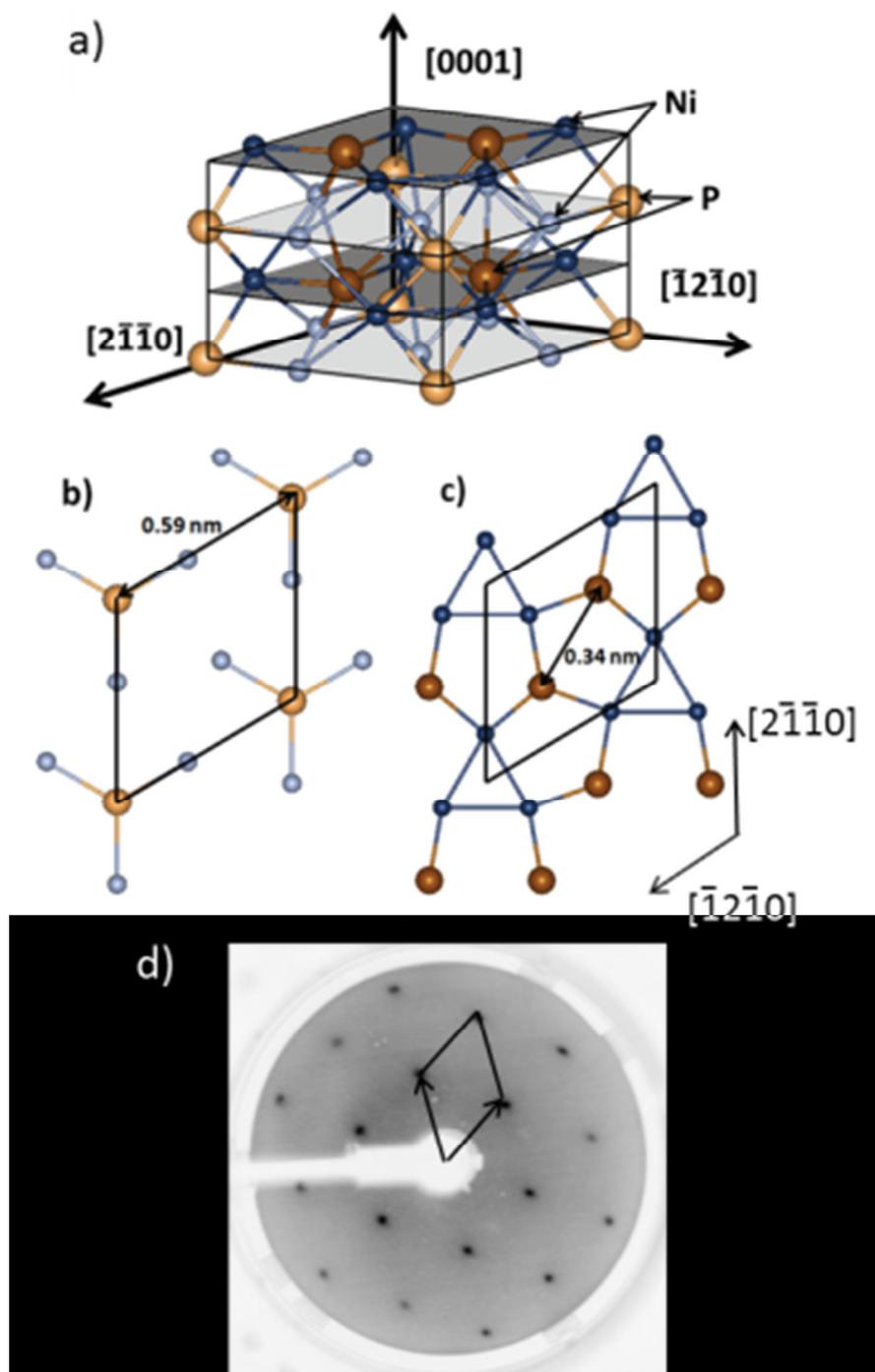
FIG. 1. a) Bulk structure of Ni_2P illustrating the alternating planes of Ni_3P and Ni_3P_2 along the [0001] direction; b) Ni_3P plane; c) Ni_3P_2 plane. Large and small balls correspond to the P and Ni atoms, respectively. d) The LEED pattern of Ni_2P (0001)-1×1 at 76 eV inserted with the reciprocal unit cell
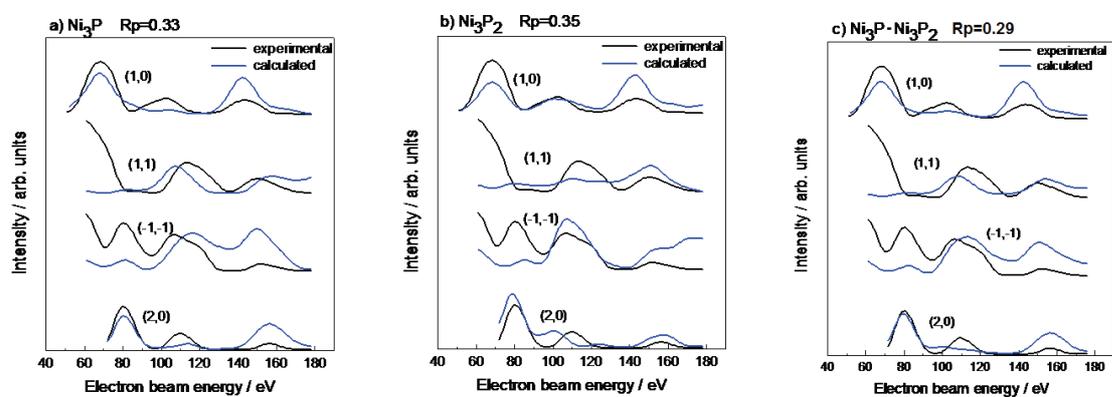
Figure

FIG. 2. Theoretical IV curves of the optimized a) Ni_3P, b) Ni_3P_2, c) two-phase Ni_3P-Ni_3P_2 (0.65:0.35) model structures compared with the experimental IV curve of Ni_2P (0001)-1×1.
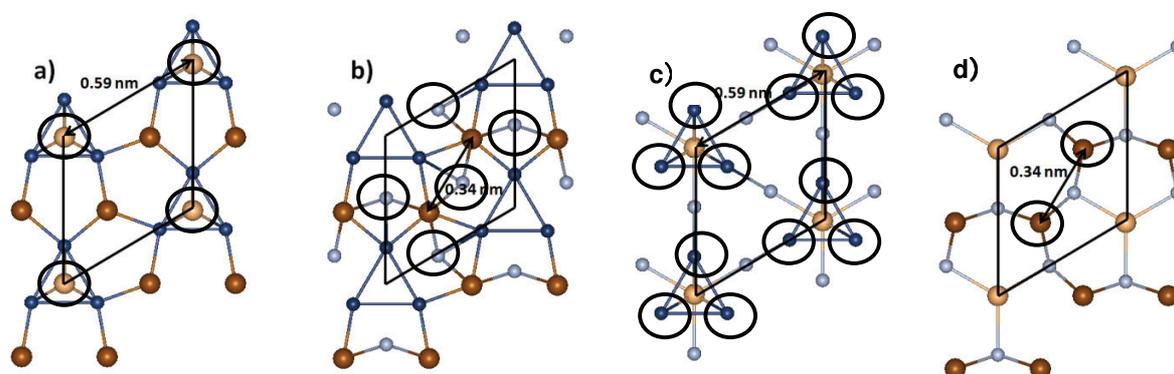
FIG. 3. The top view of the 0th and 1st layer of Ni_2P (0001)-1x1 model structures satisfying the surface space group p31m but having a different composition. a) Ni_3P_P, b) Ni_3P_Ni, c) $Ni_3P_2\_Ni$ and d) $Ni_3P_2\_P$ model structures. Circles indicated the added 0th layer atoms.
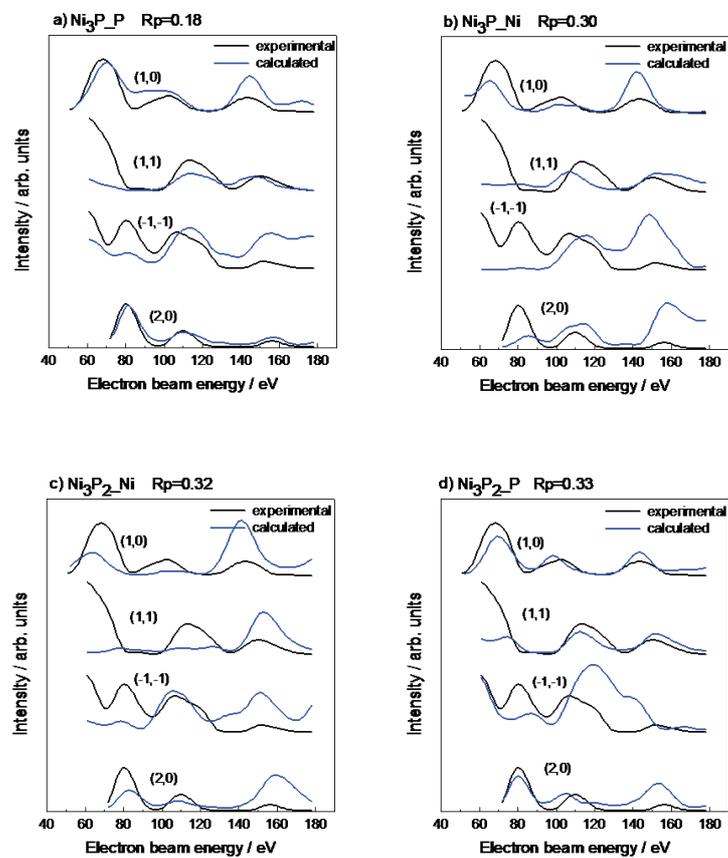
Figure

FIG. 4. Theoretical IV curves of the optimized a) Ni_3P_P, b) Ni_3P_Ni, c) $Ni_3P_2\_Ni$ and d) $Ni_3P_2\_P$ model structures compared with the experimental IV curve of Ni_2P (0001)-1×1.

Fig. 5 Alvin et al.